Coordination Solids Derived from Cp*M(CN)$_3$$^-$ (M = Rh, Ir)

Stephen M. Contakes, Kevin K. Klausmeyer, and Thomas B. Rauchfuss*

School of Chemical Sciences and the Frederick Seitz Materials Research Laboratory,
University of Illinois at Urbana−Champaign, Urbana, Illinois

Solutions of $Rh_2(OAc)_4$ and $Et_4N[Cp*Ir(CN)_3]$ react to afford crystals of the one-dimensional coordination solid $\{Et_4N[Cp*Ir(CN)_3][Rh_2(OAc)_4]\}$. This reaction is reversed by coordinating solvents such as MeCN. The structure of the polymer consists of helical anionic chains containing $Rh_2(OAc)_4$ units linked via two of the three CN ligands of $Cp*Ir(CN)_3$$^-$. Use of the more Lewis acidic $Rh_2(O_2CCF_3)_4$ in place of $Rh_2(OAc)_4$ gave purple $\{(Et_4N)_2[Cp*Ir(CN)_3]_2[Rh_2(O_2CCF_3)_4]_3\}$, whose insolubility is attributed to stronger Rh−NC bonds as well as the presence of cross-linking. The species $\{[Cp*Rh(CN)_3][Ni(en)_n](PF_6)\}$ (n = 2, 3) crystallized from an aqueous solution of $Et_4N[Cp*Rh(CN)_3]$ and $[Ni(en)_3](PF_6)_2$; $\{[Cp*Rh(CN)_3][Ni(en)_2](PF_6)\}$ consists of helical chains based on *cis*-$Ni(en)_2$$^{2+}$ units. Aqueous solutions of $Et_4N[Cp*Ir(CN)_3]$ and $AgNO_3$ afforded the colorless solid Ag-$[Cp*Ir(CN)_3]$. Recrystallization of this polymer from pyridine gave the hemipyridine adduct $\{Ag[Ag(py)][Cp*Ir-(CN)_3]_2\}$. The ^{13}C cross-polarization magic-angle spinning NMR spectrum of the pyridine derivative reveals two distinct Cp* groups, while in the pyridine-free precursor, the Cp*'s appear equivalent. The solid-state structure of $\{Ag[Ag(py)][Cp*Ir(CN)_3]_2\}$ reveals a three-dimensional coordination polymer consisting of chains of $Cp*Ir(CN)_3$$^-$ units linked to alternating Ag^+ and $Ag(py)^+$ units. The network structure arises by the linking of these helices through the third cyanide group on each Ir center.

Introduction

Solid-state organometallic compounds are a promising class of materials because their properties and structures can be manipulated using the sophisticated tools of synthetic organometallic chemistry. One recurring challenge in the area is that most solid-state organometallic materials lack manageable processing characteristics, being insoluble and infusible. These challenges have usually been met through the incorporation of solubilizing substituents, as illustrated by continuing advances in the chemistry of polymetallocenes[1] and polymetalla-alkynes.[2] In the present study, we describe a new class of organometallic solids based on μ-CN linkages and our successes in developing species with convenient solubility.

There is a long tradition of using cyanometalates in the preparation of coordination solids;[3−5] much of this tradition is rooted in the chemistry of Prussian blue.[6] The 6-fold bridging capability of the $M(CN)_6$$^{n-}$ unit leads to solids with diverse dimensionality.[7−11] There are two main advantages to the use of μ-CN linker groups. First, as illustrated by advances in high T_c magnetic materials, the μ-CN$^-$ ligand allows strong electronic coupling between the linked metal centers, in part because of the availability of both σ and π interactions with the metal centers.[12] A second advantage to the use of μ-CN linkages in the synthesis of materials comes from the fact that MCN−M

bonds are amenable to reversible cleavage, which facilitates formation of crystalline products. The sol−gel-like processing of the cyanometalates has proved useful in the development of new cyanometalate-based solids.[12,13] In the $Cp*M(CN)_3$$^-$ precursors, the Cp* ligand blocks three sites on the octahedron, which reduces the dimensionality of the polymeric derivatives and renders them particularly amenable to processing.

We have previously employed $(C_5R_5)M(CN)_3$$^-$ reagents for the preparation of molecular cages through their reactions with, inter alia, $Cp*Rh(MeCN)_3$$^{2+}$, a source of the *fac*-tritopic Lewis acid $Cp*Rh^{2+}$ (Scheme 1).[14−16] We have extended this theme to include the reactions of $(C_5Me_5)M(CN)_3$$^-$ with the electrophiles $Rh_2(O_2CR)_4$ (R = CH_3, CF_3), $Ni(en)_2$$^{2+}$, Ag^+, and Ag-$(py)^+$. These electrophiles offer diverse Lewis acid sites ranging from linear ditopic for $Rh_2(O_2CR)_4$ to trigonal pyramidal tritopic for $Ag(py)^+$. We employ both $(C_5Me_5)Rh(CN)_3$$^-$ and $(C_5Me_5)Ir-(CN)_3$$^-$. These species have very similar coordination properties, although the iridium derivatives are more robust thermally.

(1) Nguyen, P.; Gómez-Elipe, P.; Manners, I. *Chem. Rev.* **1999**, *99*, 1515−1548.
(2) Irwin, M. J.; Jia, G. C.; Vittal, J. J.; Puddephatt, R. J. *Organometallics* **1996**, *15*, 5321−5329.
(3) Iwamoto, T.; Nishikiori, S.; Kitazawa, T.; Yuge, H. *J. Chem. Soc., Dalton Trans.* **1997**, 4197−4136.
(4) Vahrenkamp, H.; Geiss, A.; Richardson, G. N. *J. Chem. Soc., Dalton Trans.* **1997**, 3643−3651.
(5) Knoeppel, D. W.; Liu, J.; Meyers, E. A.; Shore, S. G. *Inorg. Chem.* **1998**, *37*, 4828−4837.
(6) Dunbar, K. R.; Heintz, R. A. *Prog. Inorg. Chem.* **1997**, *45*, 283−391.
(7) Mironov, Y. V.; Virovets, A. V.; Artemkina, S. B.; Fedorov, V. E. *Angew. Chem., Int. Ed. Engl.* **1998**, *37*, 2507−2509.
(8) Naumov, N. G.; Virovets, A. V.; Sokolov, M. N.; Artemkina, S. B.; Fedorov, V. E. *Angew. Chem., Int. Ed. Engl.* **1998**, *37*, 1943−1945.
(9) Niu, T.; Wang, X.; Jacobson, A. J. *Angew. Chem., Int. Ed. Engl.* **1999**, *38*, 1934−1937.
(10) Lu, J. A.; Harrison, W. T. A.; Jacobson, A. J. *Chem. Commun.* **1996**, 399−400.
(11) Cernak, J.; Chomic, J.; Domiano, P.; Ori, O.; Andreeti, G. D. *Acta Crystallogr., Sect. C* **1990**, *46*, 2103.
(12) Holmes, S. M.; Girolami, G. S. *J. Am. Chem. Soc.* **1999**, *121*, 5593−5594 and references therein.
(13) Sharp, S. L.; Bocarsly, A. B.; Scherer, G. W. *Chem. Mater.* **1998**, *10*, 825−832.
(14) Klausmeyer, K. K.; Wilson, S. R.; Rauchfuss, T. B. *J. Am. Chem. Soc.* **1999**, *121*, 2705−2711.
(15) Contakes, S. M.; Klausmeyer, K. K.; Milberg, R. M.; Wilson, S. R.; Rauchfuss, T. B. *Organometallics* **1998**, *19*, 3633−3635.
(16) Klausmeyer, K. K.; Wilson, S. R.; Rauchfuss, T. B. *Angew. Chem., Int. Ed. Engl.* **1998**, *37*, 1808−1810.

Scheme 1
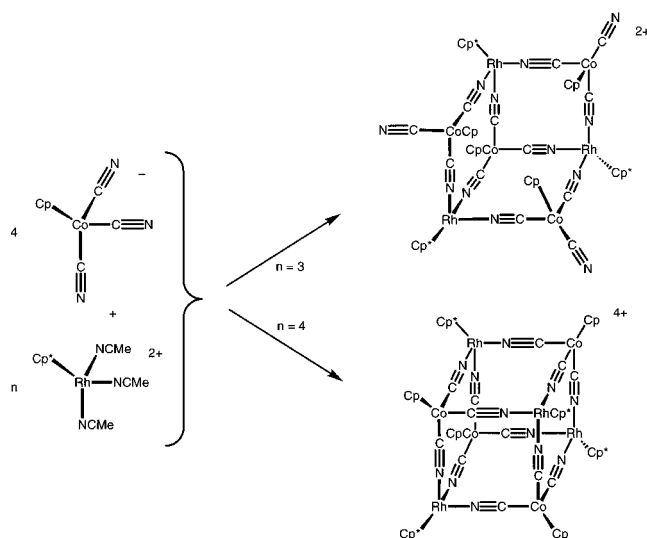
Results

Derivatives of Rh₂(O₂CR)₄. Addition of 1 equiv or more of Rh₂(OAc)₄·MeOH to stirred chloroform or acetone solutions of Et₄N[Cp*Ir(CN)₃] (**1**) resulted in an immediate color change from blue-green to purple. The ¹H NMR spectrum of the reaction mixture shows that the O₂CC*H₃* and C₅(C*H₃*)₅ signals are not shifted relative to those for free Cp*Ir(CN)₃⁻ and Rh₂-(OAc)₄. It thus appears that the interaction between **1** and the Lewis acid is weak. Over the course of 2–3 days, the reaction solution deposited purple microcrystals of the CHCl₃ solvate of {Et₄N[Cp*Ir(CN)₃][Rh₂(OAc)₄]} (**2**). The reaction is efficient (83% yield). Alternatively, **2** can be obtained more quickly but in a less crystalline state by addition of Et₂O to the reaction mixture. Compound **2** is insoluble in polar and nonpolar noncoordinating solvents but dissolves in coordinating solvents such as MeCN to give purple solutions containing free Cp*Ir(CN)₃⁻; **2** can be reprecipitated from these solutions with Et₂O (eq 1). The infrared spectrum of **2** exhibits two absorptions

$$\text{Et}_4\text{N[Cp*Ir(CN)}_3] + \text{Rh}_2(\text{OAc})_4 \underset{\text{polar solvents}}{\overset{\text{nonpolar solvents}}{\rightleftharpoons}}$$
$$\textbf{(1)}$$
$$\text{Et}_4\text{N\{[Cp*Ir(CN)}_3][\text{Rh}_2(\text{OAc})_4]\} \quad (1)$$
$$\textbf{(2)}$$
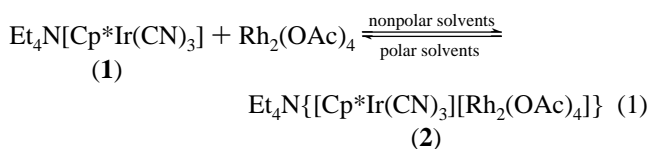
in the ν_{CN} region at 2124 and 2120 cm⁻¹.

Crystals of **2** suitable for X-ray diffraction analysis were grown by vapor diffusion of Et₂O into the CHCl₃ reaction mixture. The structure of **2** is shown in Figures 1 and 2, and selected bond lengths are given in Table 1. The compound consists of anionic helices of the formula {[Cp*Ir(CN)₃][Rh₂-(OAc)₄]⁻} together with Et₄N⁺ cations. The chains are "isotactic" because each of the Cp*Ir centers has the same stereochemistry. The Rh₂(OAc)₄ units are linked via two of the three Ir–CN ligands of Cp*Ir(CN)₃⁻, hence, the description of the anionic portion of **2** as {[Cp*Ir(μ-CN)₂CN][Rh₂(OAc)₄]⁻}∞. The asymmetric unit also contains three CHCl₃ molecules, which do not interact strongly with the polymer. The Ir–CN bond length is ca. 0.14 Å shorter for the two bridging CN than for the terminal CN. The Rh–N bond lengths of 2.180–2.232 Å are comparable to the value of 2.250 Å found for Rh₂(OAc)₄·2MeCN.[17] The C–N–Rh angles range from 159.1 to 156.7°. In Rh₂(OAc)₄·2MeCN the C–N–Rh angles are 166.9–170.1°. Jacobson has reported related but two-dimensional coordination
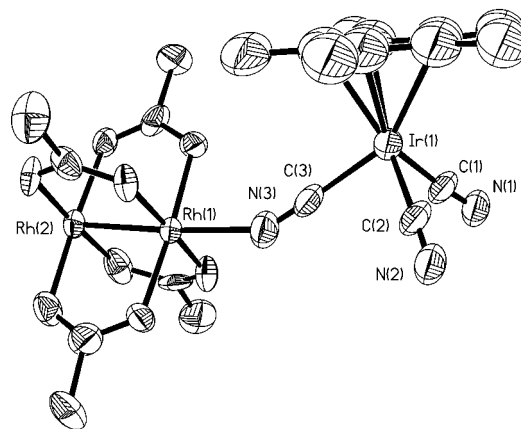
Figure 1. Anionic repeat unit in **1** with thermal ellipsoids drawn at the 50% probability level.

Table 1. Selected Bond Lengths (Å) and Angles (deg) for **2**

Rh(1)−N(3)	2.232(13)	Rh(2)−N(1)	2.180(14)
Rh(1)−Rh(2)	2.402(2)	Ir(1)−C(1)	2.02(2)
Ir(1)−C(2)	2.15(3)	Ir(1)−C(3)	2.00(2)
C(1)−N(1)	1.16(2)	C(2)−N(2)	1.10(3)
C(3)−N(3)	1.13(2)		
Rh(2)−Rh(1)−N(3)	175.6(4)	Rh(1)−Rh(2)−N(1)	177.1(4)
C(3)−N(3)−Rh(1)	151.9(14)	C(1)−N(1)−Rh(2)	156.7(14)
Ir(1)−C(1)−N(1)	174.6(15)	Ir(1)−C(2)−N(2)	178.2(23)
Ir(3)−C(3)−N(3)	175.8(15)	C(1)−Ir(1)−C(2)	89.6(6)
C(1)−Ir(1)−C(3)	89.9(6)	C(2)−Ir(1)−C(3)	89.1(7)

solids derived from Rh₂(OAc)₄ and Co(CN)₆³⁻.[10] Cotton and Felthouse have described coordination polymers where the dirhodium centers are bridged by the dibasic ligands phenazine and 2,3,5,6-tetramethylphenylenediamine.[18]

Use of Rh₂(O₂CCF₃)₄ in place of Rh₂(OAc)₄ in the above reactions led to distinctly different results. Thus, addition of 1.5 equiv Rh₂(O₂CCF₃)₄ to a stirred chloroform solution of **1** resulted in the immediate formation of a purple gel. The gel deswells upon washing with EtOH and Et₂O to give a violet glass, which analyzed as {(Et₄N)₂[Cp*Ir(CN)₃]₂[Rh₂(O₂CCF₃)₄]₃} (**3**) in 92% yield. IR measurements show a single broad absorption (fwhm = 62 cm⁻¹) in the cyanide region at 2137 cm⁻¹, the position being consistent with μ-CN ligands and the broadness being consistent with structural inhomogeneity of the μ-CN sites. In contrast to **2**, compound **3** is insoluble in coordinating solvents, including pyridine.

{[Cp*Rh(CN)₃][Ni(en)ₓ](PF₆)} (x = 2, 3). Both Et₄N-[Cp*Rh(CN)₃] and [Ni(en)₃](PF₆)₂ dissolve in water to produce homogeneous violet solutions. Such solutions deposit well-formed purple crystals analyzed to be {[Cp*Rh(CN)₃][Ni(en)₃]-(PF₆)} (**4**) along with smaller amounts of pink crystals of {[Cp*Rh(CN)₃][Ni(en)₂](PF₆)} (**5**). After 10 days, the yield of **4** was ∼30%. Crystallographic quality single crystals of both **4** and **5** grow from the reaction mixture, which is fortunate because the crystals are otherwise insoluble in common solvents and consequently are not amenable to solution-based spectroscopic analysis. The IR spectrum of **4** showed ν_{CN} bands at 2123, 2109, and 2103 cm⁻¹. That of **5** showed bands at 2140, 2130, and 2120 cm⁻¹.

Compound **4** consists of Ni(en)₃²⁺ cations linked via hydrogen bonds to Cp*Ir(CN)₃⁻ anions as shown in Figure 3. It results from simple ion exchange of Cp*Ir(CN)₃⁻ for PF₆⁻ in [Ni(en)₃]-

(17) Cotton, F. A.; Thomson, J. L. *Acta Crystallogr., Sect. B* **1981**, *37*, 2235.

(18) Cotton, F. A.; Felthouse, T. R. *Inorg. Chem.* **1981**, *20*, 600–608.
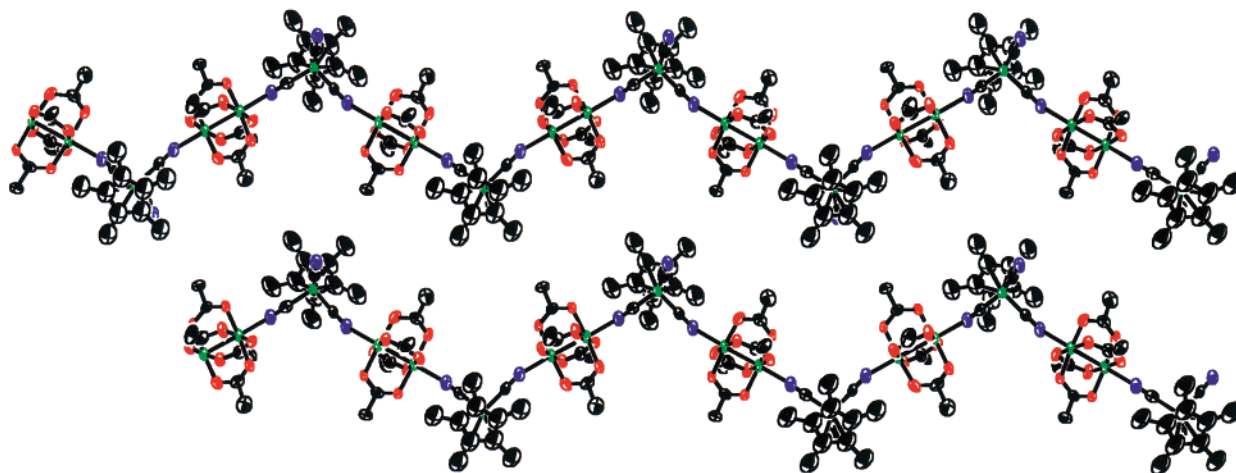
Figure 2. Structure of anionic chains of $\{[Cp^*Ir(CN)_3][Rh_2(OAc)_4]^-\}$ in **2**. Thermal ellipsoids are shown at the 50% probability level. The color labeling scheme is as follows: C, black; N, blue; O, red; Ir, green; Rh, green.

Table 2. Selected Bond Lengths (Å) and Angles (deg) for **5**

Rh(1)−C(1)	2.005(3)	Rh(1)−C(2)	1.995(3)
Rh(1)−C(3)	2.009(3)	Ni(1)−N(3)	2.093(3)
Ni(1)−N(1)	2.120(3)	C(1)−N(1)	1.154(4)
C(2)−N(2)	1.153(5)	C(3)−N(3)	1.151(4)
N(1)−Ni(1)−N(3)	95.00(11)	Ni(1)−N(1)−C(1)	146.9(3)
Ni(1)−N(3)−C(3)	167.5(3)	Rh(1)−C(1)−N(1)	172.3(3)
Rh(1)−C(2)−N(2)	176.3(3)	Rh(1)−C(3)−N(3)	174.8(3)
C(1)−Rh(1)−C(2)	86.76(13)	C(1)−Rh(1)−C(3)	86.50(12)
C(2)−Rh(1)−C(3)	92.65(13)		

$(PF_6)_2$. Aside from the fact that this species is extensively hydrogen-bonded, the molecular structure is unremarkable and is not further discussed in this report. Compound **5** formally arises via loss of en from $Ni(en)_3^{2+}$; however, attempts to convert **4** to **5** by suspending **4** in refluxing H_2O were unsuccessful. The point of interest is not the formation pathway but rather the manner by which the ditopic $Ni(en)_2^{2+}$ centers link the tricyanometalate units. The structure of the cationic portion of **5** is shown in Figures 3 and 4, while selected bond lengths and angles are presented in Table 2. The polymeric cation $\{[Cp^*Rh(CN)_3][Ni(en)_2]^+\}_n$ is well separated from the anions. As in **2**, one of the three CN ligands is nonbridging. The $Ni(en)_2^{2+}$ centers have cis-coordinated NCIr ligands. Three related $Ni(en)_2$−CN coordination solids are known.[11,19,20] In two of these, the Ni−NC ligands are exclusively cis while the third[11] contains a mixture of cis and trans. The Ni−NC distances in **5** are similar to those seen in the related solids.[11,19,20] The structure shows isotactic stereochemistry at the NC−[Cp*Ir(CN)]−CN centers. The conformation of **5** is that of a 2_1 helix with a repeat distance 7.7891 Å. There is a 1:1 mixture of right-handed helices containing Δ-$Ni(en)_2$ and left-handed helices containing Λ-$Ni(en)_2$ units.

Silver Derivatives of $Cp^*M(CN)_3^-$. The combination of aqueous solutions of **1** and $AgNO_3$ rapidly afforded a white powder of formula $Ag[Cp^*Ir(CN)_3]$ (**6**) in a process that resembles the synthesis of **3**. The infrared spectrum of **6** shows three bands at 2160, 2143, and 2115 cm^{-1}. Compound **6** is again insoluble in common solvents but does dissolve in coordinating amines. The ^1H NMR spectrum of **6** in pyridine solution shows only free $Cp^*Ir(CN)_3^-$ (δ 1.96). The IR spectrum of a pyridine solution of **6** is also identical to that for the free dianion, showing

a typical two-band ν_{CN} pattern characteristic of psuedo-C_{3v} symmetry at 2124 and 2112 cm^{-1}. These data indicate that **6** is largely dissociated in solution, as observed for **2** in MeCN. Electrospray ionization mass spectrometry (ESI-MS) measurements of solutions of **6** in pyridine show signals for $m/z = 2163$, 1648, 1135, and 622 possessing isotope patterns indicative of monocations. These data are consistent with the presence of clusters with formulas $\{[Cp^*Ir(CN)_3]_4Ag_5\}^+$, $\{[Cp^*Ir(CN)_3]_3Ag_4\}^+$, $\{[Cp^*Ir(CN)_3]_2Ag_3\}^+$, and $\{[Cp^*Ir(CN)_3]Ag_2\}^+$, respectively. The molecular structure of **6** is at present unknown; attempts to grow crystals of **6** by layering solutions of $AgNO_3$ and **1** afforded only fine powders.

The hemipyridine adduct of **6**, $\{Ag[Ag(py)][Cp^*Ir(CN)_3]_2\}$ (**7**), can be precipitated in ∼60% yield by addition of ether to pyridine solutions of **6**. The overall process relating **1** to **7** is shown in eq 2. In terms of solubility, **6** and **7** are very similar,

$$2Cp^*Ir(CN)_3^- + 2Ag^+ + py \rightarrow \{[Cp^*Ir(CN)_3]_2Ag_2py\}_n$$
$$\quad\quad (1) \quad\quad\quad\quad\quad\quad\quad\quad\quad\quad (2)$$

$$\tag{2}$$
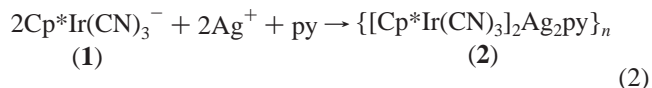
although the latter dissolves in pyridine somewhat more slowly, perhaps reflecting its greater crystallinity. The 187.5 MHz ^{13}C CP-MAS NMR spectrum of **7**, shown in Figure 5, reveals signals assigned to pyridine at δ132.4, 138.9, and 145.2 as well as two inequivalent Cp* units with signals for the CH_3 and C_5 carbon atoms at δ10.0 and 10.9 and δ98.4 and 98.9, respectively. In contrast, the corresponding spectrum for **6** has one signal each for the CH_3 and C_5 carbon atoms at δ 10.4 and 97.7, respectively, indicating that in **6** all of the Cp*Ir units are equivalent. The IR spectrum of **7** shows bands at 2147, 2126, 2108, and 2099 cm^{-1}; the complexity of the ν_{CN} portion of the IR spectrum is consistent with the relatively complicated structure of this species, which features two types of $Cp^*Ir(CN)_3^-$ subunits (*vide infra*). Aqueous solutions of $Et_4N[Cp^*Rh(CN)_3]$ and $AgNO_3$ afforded the Rh analogue of **6**, $Ag[Cp^*Rh(CN)_3]$ (**8**). The Rh−Ag compound is also soluble in pyridine.

Crystals of **7** suitable for X-ray analysis were obtained by vapor diffusion of ether into a pyridine solution of **7**. The structure of the polymer is shown in Figures 6 and 7; selected bond lengths are given in Table 3. The structure of **7** consists of an interconnected network of $Cp^*Ir(CN)_3^-$ units μ_3-bridged by Ag^+ and $Ag(py)^+$ units. In **7**, as for **2** and **5**, all cyanide ligands are bridging. The structure of **7** may be visualized as a network of interconnected helices with a backbone of the formula $\{[Cp^*Ir(CN)_2]_2[Ag][Ag(py)]\}$, which in contrast to the

(19) Ohba, M.; Fukita, N.; Okawa, H. *J. Chem. Soc., Dalton Trans.* **1997**, 1733.

(20) Ohba, M.; Maruono, N.; Okawa, H.; Enoki, T.; Latour, J.-M. *J. Am. Chem. Soc.* **1994**, *116*, 11566−11567.
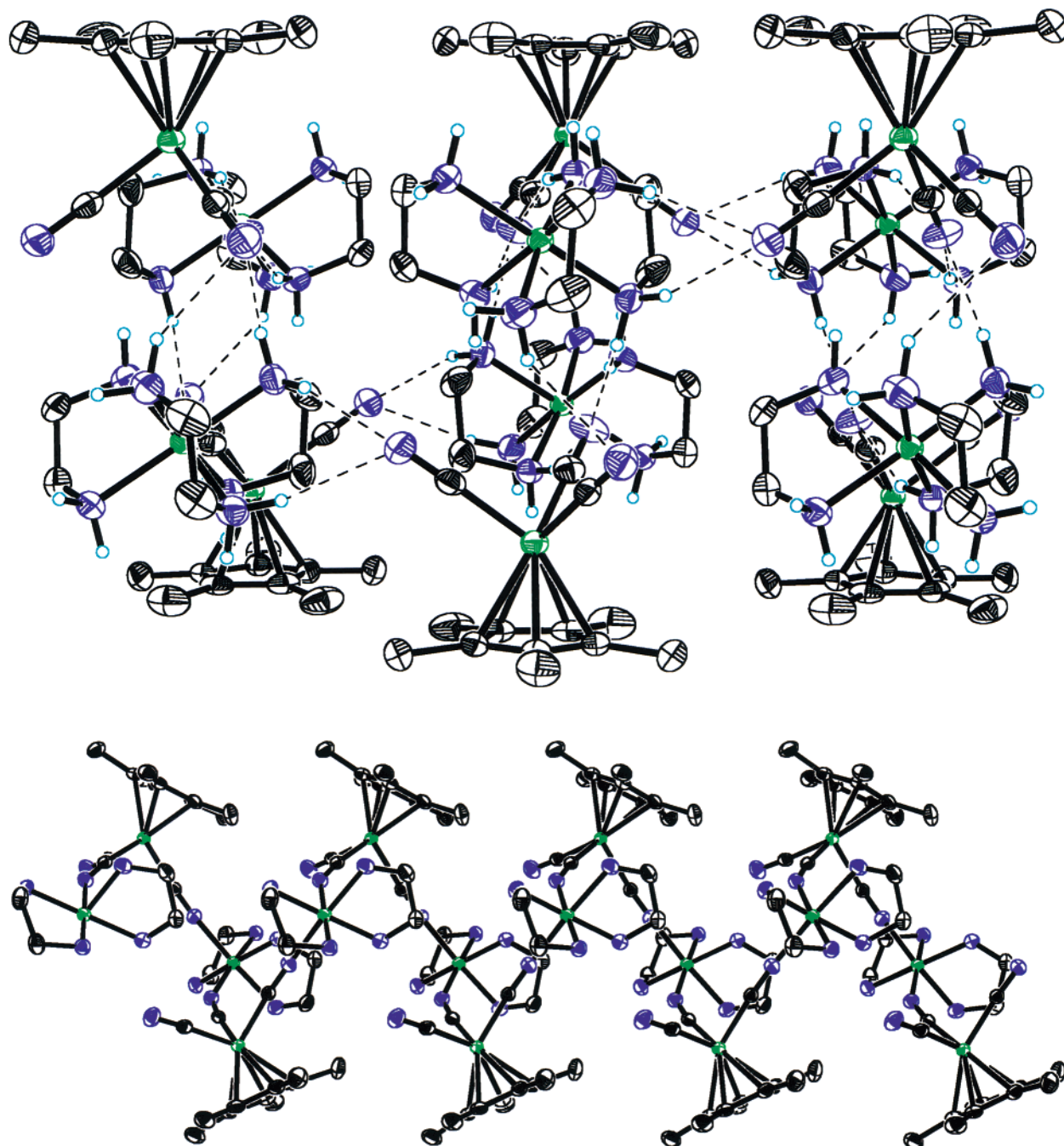
Figure 3. Top: structure of the layers in {[Cp*Rh(CN)$_3$][Ni(en)$_3$]PF$_6$} (**4**) showing the hydrogen-bonding interactions. The PF$_6^-$ ions were omitted for clarity. Bottom: structure of the cationic helical chains of {[Cp*Rh(CN)$_3$][Ni(en)$_2$]$^+$} in **5**. The color labeling scheme is as follows: C, black; N, blue; Ir, green; Ni, green. Thermal ellipsoids are shown at the 50% probability level.

polymers in **2** and **5** is charge-neutral. A portion of the network is shown in Figure 6; half of the Ag atoms are tricoordinate and half are tetracoordinate, the latter being bound to one molecule of pyridine. As a result, half of the Cp*Ir(CN)$_3^-$ units (labeled A) are bound to one Ag$^+$ and two Ag(py)$^+$ units and half (labeled B) are bound to one Ag(py)$^+$ and two Ag$^+$ units. These results are consistent with the aforementioned ^{13}C cross-polarization magic-angle spinning (CP-MAS) NMR results. The Ag–N distances range from 2.120 to 2.293 Å, the C–N–Ag-(py) angles range from 115.1 to 143.8°, and the C–N–Ag angles range from 158.1 to 172.5°. The bond distances compare favorably with literature precedents; however, the Ag–N–C(py) angles are unusually acute. Typical values are illustrated by the Ag(NCMe)$_4^+$ ion, which has Ag–N distances of 2.273 Å and C–N–Ag angles of 166.293°.[21] The helices are arranged in a

herringbone type of arrangement with cyanide units on the type A Cp*Ir(CN)$_3^-$ units bridging helixes parallel to one another and type B Cp*Ir(CN)$_3^-$ units bridging helixes in adjacent stacks.

Discussion

Half-sandwich tricyanometalates represent versatile precursors to coordination solids. Solids derived from the reaction of the tricyanometalates with the mildly Lewis acidic species Ag$^+$ and Rh$_2$(OAc)$_4$ have convenient solubility characteristics that render these species amenable to crystallization. NMR measurements on the coordination polymer {[Cp*Ir(CN)$_3$][Rh$_2$(OAc)$_4$]$^-$}$_n$

(21) Jones, P. G.; Bembenek, E. *Z. Kristallogr.* **1993**, *208*, 213.
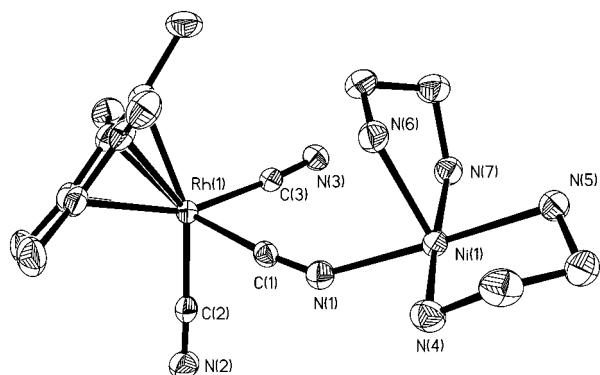
Figure 4. Cationic repeat unit in **5** with thermal ellipsoids drawn at the 50% probability level.
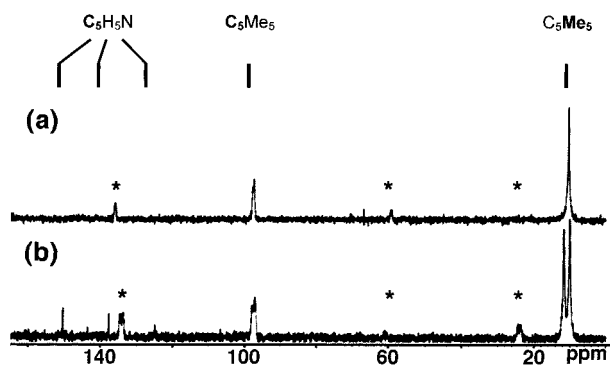
Figure 5. A 187.5 MHz ^{13}C CP-MAS NMR spectrum and peak assignments for (a) Ag[Cp*Ir(CN)$_3$] and (b) {Ag[Ag(py)][Cp*Ir-(CN)$_3$]$_2$}. Peaks marked ∗ are spinning sidebands of the C_5Me_5 signal.

confirm that the redissolution process entails "depolymerization". In order for this depolymerization−repolymerization process to be reversible, however, it is necessary that the solvent be coordinating but not strongly so. On the other hand, adducts derived from Rh$_2$(O$_2$CCF$_3$)$_4$ and Ni(en)$_2^{2+}$ are insoluble and cannot be recrystallized even using strong donor solvents. The insolubility of these latter materials is attributed to the enhanced Lewis acidity of the precursor Ni- and Rh-containing reactants and the resulting greater strength of the M−NC bond. The highly Lewis acidic nature of the fluorinated dirhodium species has been clearly demonstrated.[22,23] The strengthened M−N linkages in these solids is borne out by the infrared spectral data; in the Rh$_2$(OAc)$_4$ adduct, **2**, two ν_{CN} bands are observed, whereas the Rh$_2$(O$_2$CCF$_3$)$_4$ derived solid has a single band at 2137 cm^{-1}, indicative of a stronger C≡N and, by implication, M−N bond.[6,24] Linear polymers of the type {[Cp*M(CN)(μ-CN)$_2$]-[M$_m$L$_n$]^z}$_o$ (e.g., **2** and **5**) can adopt two regular connectivities: isotactic and syndiotactic. We only observe the former. It is well-known that Ni(amine)$_4^{2+}$ centers are effective precursors to polymeric solids containing the linkage MCN···Ni···NCM.[25] In our study, the *cis*-Ni(en)$_2^{2+}$ unit engages the Cp*M(CN)$_3^-$ unit to give a polymer following the pattern seen for the Cp*Ir(CN)$_3^-$ adduct of the 2-connecting Rh$_2$(OAc)$_4$.

Studies using Ag$^+$-derived polymers were especially revealing. The success of the repolymerization−crystal growth is attributed to the ability of the pyridine to compete with μ-CN

(22) Cotton, F. A.; Dikarev, E. V.; Stiriba, S.-E. *Organometallics* **1999**, *18*, 2724−2726.
(23) Telser, J.; Drago, R. S. *Inorg. Chem.* **1986**, *25*, 2989−2992.
(24) Nakamoto, K. *Infrared and Raman Spectra of Inorganic and Coordination Compounds*; John Wiley: New York, 1986.
(25) Mallah, T.; Auberger, C.; Verdaguer, M.; Veillet, P. *J. Chem. Soc., Chem. Commun.* **1996**, 61−62.

Table 3. Selected Bond Lengths (Å) and Angles (deg) for **7**

Ag(1)−N(3)	2.266(7)	Ag(1)−N(2)	2.283(7)
Ag(1)−N(5)	2.293(7)	Ag(1)−N(7)	2.415
Ag(2)−N(1)	2.185(6)	Ag(2)−N(4)	2.120(8)
Ag(2)−N(6)	2.283(8)	C(1)−N(1)	1.156(10)
C(2)−N(2)	1.160(10)	C(3)−N(3)	1.147(10)
C(14)−N(4)	1.143(10)	C(15)−N(5)	1.144(9)
C(16)−N(6)	1.193(11)	Ir(1)−C(1)	1.980(9)
Ir(1)−C(2)	1.992(8)	Ir(1)−C(3)	1.998(9)
Ir(2)−C(14)	2.020(9)	Ir(2)−C(15)	2.000(8)
Ir(2)−C(16)	1.963(10)		
N(3)−Ag(1)−N(2)	116.4(3)	N(3)−Ag(1)−N(5)	110.4(2)
N(2)−Ag(1)−N(5)	129.2(2)	N(3)−Ag(1)−N(7)	106.5(3)
N(2)−Ag(1)−N(7)	91.6(3)	N(5)−Ag(1)−N(7)	93.1(3)
N(4)−Ag(2)−N(1)	141.1(3)	N(4)−Ag(2)−N(6)	118.5(3)
N(1)−Ag(2)−N(6)	100.2(3)	C(1)−N(1)−Ag(2)	158.1(7)
C(14)−N(4)−Ag(2)	172.5(7)	C(16)−N(6)−Ag(2)	162.9(7)
C(2)−N(2)−Ag(1)	143.7(7)	C(3)−N(3)−Ag(1)	159.5(7)
C(15)−N(5)−Ag(1)	143.8(6)	NC−Ir(1)−CN (av)	89.2
NC−Ir(2)−CN (av)	92.3	Ir(1)−C-N (av)	180.3
		Ir(2)−C-N (av)	172.2
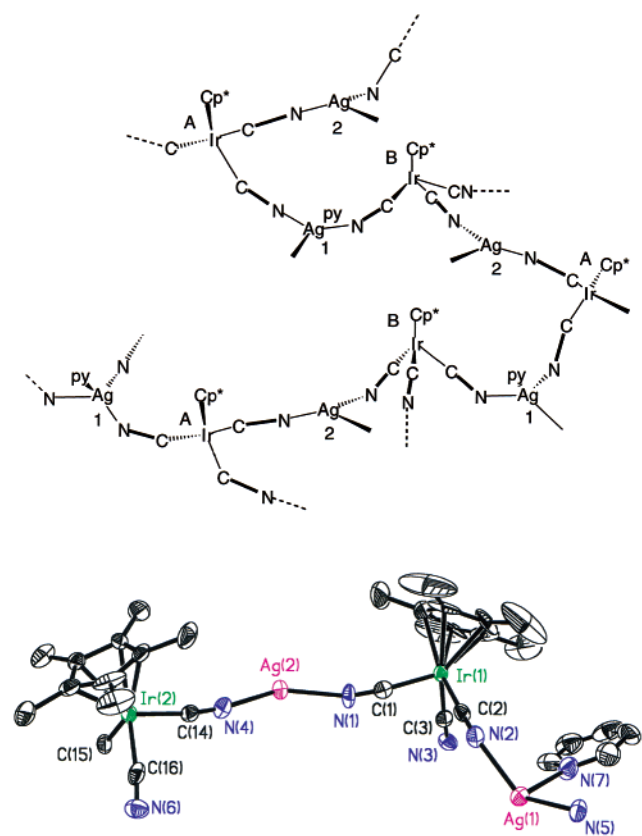
Figure 6. Top: portion of the helix structure of **7** showing the two different types of Cp*Ir(CN)$_3^-$ units. The Ir(B) units are bridged to two trigonal planar Ag(1) and one tetrahedral Ag(2). The Ir(A) units are bridged to two Ag(1) and one Ag(2). Bottom: asymmetric unit of **7** showing the atom labeling scheme. Thermal ellipsoids are drawn at the 50% probability level. The coloring scheme is as follows: C, black; N, blue; Ir, green; Ag, purple.

ligands. Apparently, the preference of Ag$^+$ for py vs IrC*N* is such that the only a small amount of the pyridine remains coordinated upon crystallization. It is interesting to note that in the resulting solid, all CN ligands are bridging; thus, the degree of cross-linking is maximized in contrast to the two other structurally characterized solids presented in this paper.

In this work we employed three very different linker groups, Ag$^+$, Rh$_2$(OAc)$_4$, and Ni(en)$_2^{2+}$. Many other linker groups could be envisioned, and we have recently reported the synthesis of organometallic sheet-like solids derived from the interaction of

Figure 7. Structure of {Ag[Ag(py)][Cp*Ir(CN)$_3$]$_2$} (**7**) with thermal ellipsoids drawn at the 50% probability level. The coloring scheme is as follows: C, black; N, blue; Ir, green; Ag, purple.

Table 4. Details of Data Collection and Structure Refinement for the Complexes **2**, **5**, and **7**

	2	**5**	**7**
chemical formula	C$_{32}$H$_{50}$Cl$_9$IrN$_4$O$_8$Rh$_2$	C$_{17}$H$_{31}$F$_6$N$_7$NiPRh	C$_{31}$H$_{35}$Ag$_2$Ir$_2$N$_7$
cryst size (mm)	0.14 × 0.8 × 0.03	0.48 × 0.46 × 0.20	0.14 × 0.12 × 0.10
space group	P2$_1$2$_1$2$_1$	P2$_1$/c	P2$_1$2$_1$2$_1$
a (Å)	13.2631(5)	15.3435(2)	8.60860(10)
b (Å)	18.3666(6)	7.789	13.4156(3)
c (Å)	20.5855(7)	20.6625(3)	28.6587(6)
β (deg)	90	92.7920	90
V (Å^3)	5014.6(3)	2466.49(5)	3309.78(11)
Z	4	4	4
D_{calcd} (Mg m^{-3})	1.746	1.724	2.219
μ (Mo Kα, mm^{-1})	3.795	1.562	9.213
min & max transm	0.8407−0.9963	0.657−0.969	0.7626−0.9871
reflns measd	26 694	15 446	21 872
independent reflns	8817	5850	7705
R_{int}	0.1264	0.0233	0.0507
R1 [$I > 2\sigma$] (all data)	0.0626 (0.1490)	0.0406 (0.0458)	0.0316 (0.0468)
wR2 [$I > 2\sigma$] (all data)	0.1295 (0.1505)	0.0886 (0.0896)	0.0620 (0.0646)

Cp*Ir(CN)$_3^-$ with H$_3$O$^+$.[26] Additionally, the tritopic tricyanide could be varied in many ways, an obvious approach being the use of other facial ligands.[27] It should also be possible to employ linker ligands other than CN$^-$.

Experimental Section

Materials and Methods. The preparation of Et$_4$N[Cp*Rh(CN)$_3$],[16] Rh$_2$(OAc)$_4$,[28] and Rh$_2$(O$_2$CCF$_3$)$_4$[28] followed literature procedures. For the trifluoroacetate, 20 cycles of dissolution and evaporation using 10 mL of CF$_3$CO$_2$H each were used instead of 4 cycles with 25 mL of

(26) Contakes, S. M.; Schmidt, M.; Rauchfuss, T. B. *Chem. Commun.* **1999**, 1183−1184.
(27) Heinrich, J. L.; Berseth, P. A.; Long, J. R. *Chem. Commun.* **1998**, 1231−1232.
(28) Johnson, S. A.; Hunt, H. R.; Neumann, H. M. *Inorg. Chem.* **1963**, *2*, 960−962.

CF$_3$CO$_2$H. This was necessary to ensure complete substitution of CF$_3$CO$_2^-$ for OAc$^-$. The purity of the Rh$_2$(O$_2$CCF$_3$)$_4$ was established by ^{19}F NMR spectroscopy (400 MHz, CD$_3$CN: δ −75.948). Deuterated solvents for NMR work were obtained from Cambridge Isotope Labs and used without further purification. Trifluoromethanesulfonic acid (98% HOTf) and AgNO$_3$ (99+%) were obtained from Aldrich and used without further purification. All solvents were obtained from Fischer as reagent grade materials and used without further purification.

{Et$_4$N[Cp*Ir(CN)$_3$][Rh$_2$(OAc)$_4$]·3CHCl$_3$} (2). A solution of 53.5 mg (0.100 mmol) of Et$_4$N[Cp*Ir(CN)$_3$] in 5 mL of CHCl$_3$ was added to a suspension of 51 mg (0.100 mmol) of Rh$_2$(OAc)$_4$·2MeOH in 5 mL of CHCl$_3$. When mixed, the Rh$_2$(OAc)$_4$·2MeOH dissolved to give a blue solution. The reaction solution was diluted with 30 mL of Et$_2$O to precipitate purple microcrystals. The product was collected by filtration, washed with two 10 mL portions of Et$_2$O, and dried under vacuum for 3 h. Yield: 110 mg (83%). IR (KBr): ν_{CN} = 2124, 2120 cm^{-1}. ^{1}H NMR (500 MHz, CD$_3$CN): δ 1.757 (O$_2$CCH$_3$), 1.999 (C$_5$-

Me$_5$). Anal. Calcd for C$_{32}$H$_{50}$Cl$_9$IrN$_4$O$_8$Rh$_2$: C, 28.77; H, 3.77; N, 4.19. Found: C, 28.96; H, 3.82; N, 3.83.

{(Et$_4$N)$_2$[Cp*Ir(CN)$_3$]$_2$[Rh$_2$(OCCF$_3$)$_4$]$_3$} (3). A solution of 27 mg (0.50 mmol) of Et$_4$N[Cp*Ir(CN)$_3$] in 5 mL of CHCl$_3$ was added to a solution of 50 mg (0.76 mmol) of Rh$_2$(OCCF$_3$)$_4$ in 5 mL of CHCl$_3$. When mixed, a purple gelatinous solid immediately forms. This was collected by filtration and washed with two 10 mL portions each of EtOH followed by Et$_2$O. During these washings, the gelatinous solid deswelled to become a dark-purple glassy solid. The product was dried under vacuum for 6 h. Yield: 71 mg (92%). IR (KBr): ν_{CN} = 2137 cm^{-1}. Anal. Calcd for C$_{66}$H$_{70}$F$_{36}$Ir$_2$N$_8$Rh$_6$: C, 26.03; H, 2.32; N, 3.68; F, 22.46; Ir, 12.62; Rh, 20.28. Found: C, 25.95; H, 2.47; N, 3.47; F, 22.34; Ir, 12.56; Rh, 18.48.

{[Cp*Rh(CN)$_3$][Ni(en)$_x$](PF$_6$)} (4 and 5). A solution of 100 mg (0.224 mmol) of Et$_4$N[Cp*Rh(CN)$_3$] in 20 mL of H$_2$O was added dropwise to a solution of 178 mg (0.336 mmol) of [Ni(en)$_3$](PF$_6$)$_2$ in 20 mL of H$_2$O with stirring. The resulting clear purple solution was allowed to stand (unstirred) for 10 d during which time purple crystals appeared. The crystals were removed manually, washed with two 5 mL portions of H$_2$O, and dried in a stream of nitrogen for 4 h. Yield of **4**: 48 mg (31%). IR (KBr): ν_{CN} = 2123, 2109, 2103 cm^{-1}. Anal. Calcd for C$_{25}$H$_{39}$F$_6$N$_9$NiPRh: C, 31.78; H, 5.75; N, 17.55. Found: C, 31.78; H, 5.69; N, 17.57. A small amount of pink crystals of **5** were found floating on the aqueous solution. The crystals of **5** were selected individually, washed with H$_2$O, and dried in a stream of N$_2$. IR (KBr): ν_{CN} = 2140, 2130, 2110 cm^{-1}.

{Ag[Cp*Ir(CN)$_3$]} (6). A solution of 107 mg (0.200 mmol) of Et$_4$N-[Cp*Ir(CN)$_3$] in 5 mL of H$_2$O was added to a solution of 34 mg (0.200 mmol) of AgNO$_3$ in 10 mL of H$_2$O with stirring. A white powder precipitated immediately. The product was collected by filtration, washed with two 10 mL portions each of acetone and Et$_2$O, and dried under vacuum for 12 h. Yield: 87 mg (85%). IR (KBr): ν_{CN} = 2160, 2143, 2127, 2109, 2099 cm^{-1}. ^{1}H NMR (500 MHz, C$_5$D$_5$N): δ 1.961 (C$_5$Me$_5$). ^{13}C CP-MAS NMR (187.5 MHz): δ 10.431 (C$_5$*Me$_5$), 97.648 (*C*$_5$Me$_5$). ESI-MS (pyridine, *m/z*): 621.9 ({[Cp*Ir(CN)$_3$]Ag$_2$}$_x^{x+}$), 1134.6 ({[Cp*Ir(CN)$_3$]$_2$Ag$_3$}$_x^{x+}$), 1647.9 ({[Cp*Ir(CN)$_3$]$_3$Ag$_4$}$_x^{x+}$), 2161 ({[Cp*Ir(CN)$_3$]$_4$Ag$_5$}$_x^{x+}$). Anal. Calcd for C$_{13}$H$_{15}$AgIrN$_3$O: C, 29.38; H, 3.22; N, 7.91. Found: C, 29.31; H, 2.77; N, 7.73.

{Ag[Ag(py)][Cp*Ir(CN)$_3$]$_2$} (7). A solution of 51 mg (0.10 mmol) of {Ag[Cp*Ir(CN)$_3$](H$_2$O)} in 2 mL of pyridine was filtered to remove traces of an insoluble impurity. Then 2.5 mL of CHCl$_3$ followed by 10 mL of Et$_2$O was added to precipitate the product as a white powder.

Yield: 43 mg (61%). IR (KBr): ν_{CN} = 2147, 2126, 2108, 2099 cm^{-1}. ^{1}H NMR (500 MHz, C$_5$D$_5$N): δ 1.961 (C$_5$Me$_5$). ^{13}C CP-MAS NMR (187.5 MHz, solid state): δ 11.673, 10.081 (C$_5$*Me$_5$), 97.850, 97.144 (*C*$_5$Me$_5$), 150.320, 137.705, 124.935 (*C*$_5$H$_5$N). Anal. Calcd for C$_{31}$H$_{35}$-Ag$_2$Ir$_2$N$_7$: C, 33.67; H, 3.19; N, 8.87. Found: C, 33.89; H, 3.22; N, 8.73.

{Ag[Cp*Rh(CN)$_3$]} (8). A solution of 89 mg (0.200 mmol) of Et$_4$N-[Cp*Rh(CN)$_3$] in 5 mL of H$_2$O was added to a solution of 34 mg (0.200 mmol) of AgNO$_3$ in 5 mL of H$_2$O with stirring to immediately precipitate a white powder. The product was collected by filtration, washed with two 10 mL portions each of acetone and Et$_2$O, and dried under vacuum for 12 h. Yield: 74 mg (87%). IR (KBr) ν_{CN} = 2157, 2146, 2125, 2113, 2105 cm^{-1}. ^{1}H NMR (500 MHz, C$_5$D$_5$N): δ 1.890 (C$_5$Me$_5$). ESI-MS (pyridine, *m/z*): 531.9 ([Cp*Rh(CN)$_3$]Ag$_2^+$), 956.8 ([Cp*Rh(CN)$_3$]$_2$Ag$_3^+$). Anal. Calcd for C$_{13}$H$_{15}$AgN$_3$Rh: C, 36.82; H, 3.57; N, 9.91. Found: C, 36.72; H, 3.63; N, 10.08.

X-ray Data Collection and Structure Refinement. Crystals of **2**, **5**, and **7** were mounted on a thin glass fiber using oil (Paratone-N, Exxon) before being transferred to the diffractometer. The data were collected on a Siemens Platform/CCD automated diffractometer at 198 K. All data processing was performed with the integrated program package SHELXTL.[29] All structures were solved using direct methods and refined using full matrix least squares on F^2 using the program SHELXL-93.[30] Hydrogen atoms were fixed in idealized positions with thermal parameters 1.5 times those of the attached carbon atoms. The data were corrected for absorption on the basis of Ψ scans. Further details are given in Table 4.

Supporting Information Available: Tables of atomic coordinates, selected bond distances and angles, and thermal parameters. This material is available free of charge via the Internet at http://pubs.acs.org.

IC991037R

(29) Sheldrick, G. M. SAINT, version 5, and SHELXTL, version 5, Bruker AXS, 1998.
(30) Sheldrick, G. M. *SHELXL-97*; University of Göttingen: Germany, 1997.